

Accurate Ranging in a Stratified Underwater Medium with Multiple Iso-gradient Sound Speed Profile Layers

Hamid Ramezani*, Geert Leus*

*Faculty of Electrical Engineering, Mathematics and Computer Science
Delft University of Technology (TU Delft)
e-mail:{h.mashhadiramezani, g.j.t.leus}@tudelft.nl

Abstract: Most of the available localization algorithms require pair-wise ranging between the nodes. The more accurate the ranging, the more precise the localization. In this paper, the problem of accurate ranging between sensor nodes in an underwater environment is considered. It is assumed that the underwater medium is composed of layers with an isogradient depth-dependent sound speed profile (SSP). For the range estimation, we first show how the pair-wise time of flight (ToF) measurement between the nodes is related to the nodes' positions. Then, based on this relation, we propose a novel ranging algorithm for an underwater acoustic sensor network (UASN). The proposed algorithm is based on the ToF measurement of the first arrival ray which may be reflected from the surface or the seabed. Through several simulations we show that the algorithm performs superb, and meets the Cramér Rao bound (CRB) for different values of the measurement noise power.

Keywords: Localization, ranging, sound speed profile, ray tracing, underwater acoustic sensor networks.

1. INTRODUCTION

Underwater localization is very challenging; very low bit rate, low link quality, multi-path, and time variability are the most challenging characteristics of underwater communications [1]. In addition, the propagating wave speed in an underwater environment, is not constant, and depends on the location. In such a medium, the time of flight (ToF) between two nodes depends not only on the sound speed profile (SSP) of that medium but also on the position of the two nodes [2]. Therefore, the ToF is not only proportional to the Euclidean distance between the nodes, but also to their positions. However, it can be shown that in an underwater medium where the SSP varies only with depth, the ToF can be used to estimate the distance between the nodes if the nodes' depth is known.

The sensor nodes of a UASN can be equipped with a pressure sensor and thus are capable to measure their depth. It is proved that in a three dimensional (3D) environment using depth information, only horizontal distances between the nodes are required for localization [3]. To find a horizontal distance between two nodes using ToF measurements we can build a look up table (LUT) which relates the ToF to the horizontal distance between two nodes [4]. Using this approach to estimate mutual distances between nodes from ToF measurements, is quite fast, but to scan the whole underwater environment, a huge LUT is required which may not be practical. Furthermore, the SSP in an underwater medium is

subject to changes in temperature and conductivity, and any change in SSP degrades the LUT accuracy and upsets the localization performance.

In this work, we analyze the acoustic signal propagation between two sensor nodes in an underwater environment. We use a ray-tracing approach to model the propagation which is a valid approximation for high-frequency signal transmission [4]. We assume that the underwater medium is composed of different layers with an iso-gradient SSP, which is a practical model for the actual SSP of the entire environment [5], [6]. We will show that the positions of the crossing points, where the ray trajectory and the layer boundaries meet each other, can be obtained through a set of polynomial root finding equations. Based on these equations we are able to distinguish among different possible transmission paths between the nodes, and determine the fastest one even if it is reflected from the sea surface or the seabed. Another contribution of this paper is a novel method for accurate ranging between the nodes. The proposed algorithm computes the horizontal distance between two nodes based on the ToF and depth measurements. The algorithm estimates the range of a target by minimizing the difference between the measured ToF and the constructed ToF estimated from the known map in an iterative manner.

The rest of the paper is organized as follows. The ToF versus node positions is computed in Section 2. In Section 3, we propose our ranging algorithm, and through several simulations we evaluate its performance in Section 4. Finally, we conclude the paper in Section 5.

2. TOF VERSUS NODES' POSITIONS

In order to relate the ToF to the unknown node's position, we first require to find which ray departing the source reaches a specific destination. In this section, we analytically find the rays that can travel between two nodes with known positions, and we compute their corresponding ToFs based on their trajectories. It is worth mentioning that in an underwater medium with fixed SSP, each ray departing a source can be uniquely characterized by its departing angle.

Here the SSP is considered as a piece-wise linear function of the depth:

$$c^{(j)}(z) = a^{(j)}z + b^{(j)}, \quad z^{(j-1)} < z < z^{(j)}, \quad j \in 1, \dots, N, \quad (1)$$

where z represents the depth, $a^{(j)}$ and $b^{(j)}$ are related to the chemical and physical characteristics of the j -th isogradient sound speed profile layer, and N is the number of layers. In our previous work [7], we show how a ray can travel between two nodes located inside an iso-gradient SSP underwater environment. We review this work first for completeness.

A. Single-Layer Medium

In a single layer, each truncated ray (indexed by p) between two points, i.e., S_p and E_p in Fig. 1, can be uniquely characterized if the position of the starting point, position of the end point, and SSP are known. The function between the layer index and truncated ray index is given by $j(p)$, and for ease of notation, we define

$$c_p(z) = a_p z + b_p = c^{(j(p))}(z) = a^{(j(p))}z + b^{(j(p))}. \quad (2)$$

The relation between ToF and the node positions can then be extracted from a set of differential equations characterized by Snell's law [4],

$$\frac{\cos \theta}{c_p(z)} = \frac{\cos \theta_p^S}{c_p(z_p^S)} = \frac{\cos \theta_p^E}{c_p(z_p^E)} = k_0, \quad \text{and } \theta \in \left(\frac{-\pi}{2}, \frac{\pi}{2} \right), \quad (3)$$

where θ_p^S and θ_p^E are the ray angles at the starting and end points, respectively, z_p^S and z_p^E represent the depth of the starting and end node, respectively, and k_0 is constant along a ray traveling between the nodes (see Fig. 1). Moreover, the parameters θ and z represent the angle and depth of a given point along the ray. Now, we can write

$$\partial r = \frac{\partial z}{\tan \theta}, \quad (4a)$$

$$\partial s = \frac{\partial z}{\sin \theta}, \quad (4b)$$

$$\partial t = \frac{\partial s}{c_p(z)}, \quad (4c)$$

where s is the arc length of a ray traveling between the two nodes, and t is its corresponding travel time. From (2) and (3), by taking derivatives w.r.t. z and θ , we can write

$$\partial z = -\frac{1}{a_p k_0} \sin \theta \partial \theta. \quad (5)$$

Using the above differential equations, for the two points

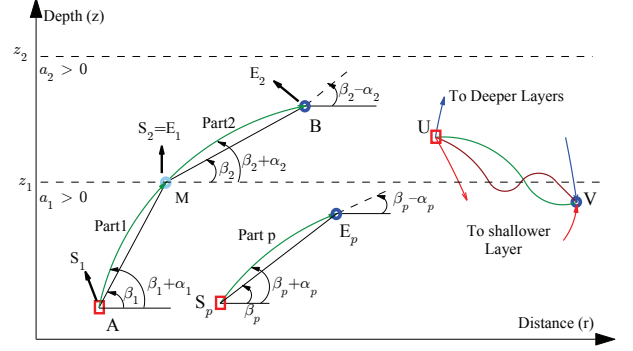


Fig. 1. Samples of ray trajectories as they travel through different layers

we have [7]

$$r_p^E - r_p^S = \sqrt{(x_p^E - x_p^S)^2 + (y_p^E - y_p^S)^2}, \quad (6a)$$

$$X_p = \frac{z_p^E - z_p^S}{r_p^E - r_p^S}, \quad (6b)$$

$$Y_p = \begin{cases} \frac{K_p}{X_p}, & z_p^S \neq z_p^E \\ \frac{0.5a_p(r_p^E - r_p^S)}{b_p + a_p z_p^S}, & z_p^S = z_p^E \end{cases} \quad (6c)$$

$$K_p = \frac{0.5a_p(z_p^E - z_p^S)}{b_p + 0.5a_p(z_p^E + z_p^S)}, \quad (6d)$$

$$\tan \beta_p = X_p, \quad (6e)$$

$$\tan \alpha_p = Y_p, \quad (6f)$$

$$\theta_p^S = \beta_p + \alpha_p, \quad (6g)$$

$$\theta_p^E = \beta_p - \alpha_p, \quad (6h)$$

$$t_p = \frac{-1}{a_p} \left[\ln \frac{1 + \sin \theta_p^E}{\cos \theta_p^E} - \ln \frac{1 + \sin \theta_p^S}{\cos \theta_p^S} \right], \quad (6i)$$

where $r_p^E - r_p^S$ is the horizontal distance between the points, $\mathbf{x}_p^S = [x_p^S, y_p^S, z_p^S]^T$ and $\mathbf{x}_p^E = [x_p^E, y_p^E, z_p^E]^T$ are the coordinates of the starting and end points, respectively, and t_p is the traveling time of a truncated ray between these two nodes. Note that β_p represents the angle of the straight line connecting the nodes w.r.t. the horizontal axis, and α_p is the angle between the actual ray and this straight line. From (6g) and (6h), it can be seen that the ray deviations from the straight line at the starting and end point are the same but have opposite signs.

B. ToF Versus Node Positions for Two Adjacent Layers

We start our analysis by considering a ray traveling between two points in adjacent layers, i.e., the ray from A to B in Fig. 1. In this scenario, when the r coordinate of the crossing point, M, is computed, we are able to relate the positions of the two nodes to the ToF. The ray has two parts; the ending point of the first part is the starting point of the second part. Thus, the two parts of the ray can be related to each other according to a boundary equation $\theta_2^S = \theta_1^E$. Another representation for this boundary equation can be obtained by taking the tangent from both sides. Using (6e) to (6h), the boundary equation can then be modified to

$$\frac{X_2 + Y_2}{1 - K_2} = \frac{X_1 - Y_1}{1 + K_1}. \quad (7)$$

For a two-part ray, the combination of sub-equations (6b), (6c), and (6d) for each part, together with boundary equation (7)

forms a third-order polynomial root finding problem where the roots represent the possible r coordinates of the crossing point M. Notice that the node positions and the depth of M are known and as a result, the parameters K_1 and K_2 can be computed easily, X_1 (X_2) is inversely related to Y_1 (Y_2), and the only unknown parameter is r^M which determines X_1 and X_2 . Since there are at most three roots for a third order polynomial, there are at most three ways for a ray departing at A to reach B. In the next subsections we show how the ToF can be computed for a multi-part ray. Note that, as illustrated in Fig. 1, there are many other ways that a ray may travel between two points in adjacent layers, i.e., U to V in Fig. 1. An analysis of all possible rays is feasible, and we will later on discuss this.

C. Definition of Ray Pattern

To simplify the multi-layer analysis, we define the concept of *ray pattern*. A ray pattern is a set, consisting of all possible rays that can travel between two points according to a specific pattern. For example, a ray pattern of 2.1.1.2 means that, the ray departs the starting point from the second layer, goes to the first layer, hits the surface, and arrives to the second node in the second layer. Therefore, a *ray pattern* has several properties. First, the number of digits used in the *ray pattern* indicates the number of single-layer parts a ray consists of. Second, it shows in which layer each part of a ray is located. Third, the reflection from the sea surface and the seabed can easily be modeled by this concept. Using the *ray pattern* concept, we are able to show how a ray can travel in a given medium, and which pattern may host the fastest ray.

D. Ray Tracing in a Multilayer Medium

To predict how a ray may travel inside a multi-layer underwater area we introduce several lemmas bellow.

Lemma 1: In a layer with constant SSP the ToF is related to the nodes' positions as $t_p = \frac{1}{b_p} \sqrt{(r_p^E - r_p^S)^2 + (z_p^E - z_p^S)^2}$.

Lemma 2: Rays are bent toward the region where the sound speed is lower.

Lemma 3: In a layer, the depth along a truncated ray between two points, S_p and E_p , can exceed the region $[z_p^S, z_p^E]$ if and only if (iff) the sign of $\theta_p^S \theta_p^E$ is negative. The excess value can be computed as,

$$\Delta z = \begin{cases} \frac{a_p z_p^S + b_p}{a_p \cos \theta_p^S} (1 - \cos \theta_p^S), & \text{if } |\theta_p^S| < |\theta_p^E| \\ \frac{a_p z_p^E + b_p}{a_p \cos \theta_p^E} (1 - \cos \theta_p^E), & \text{if } |\theta_p^S| > |\theta_p^E| \end{cases} \quad (8)$$

In this way, it can be understood that if Δz for a one-part ray in a single layer is so large that a ray part crosses another layer, the assumption of a one-part ray propagation has to be changed into a three-part ray propagation, and the equations have to be reorganized accordingly.

Lemma 4: A ray can travel multiple times between two layers if the SSP has a local minimum between them.

Lemma 5: Reflections from the seabed and sea surface can be formulated as a boundary equation. For instance, if we consider a perfect reflection from the seabed or the sea surface,

the boundary equations can be obtained as

$$\begin{aligned} \beta_{p+1} + \alpha_{p+1} &= -(\beta_p - \alpha_p), \\ \beta_{p+1} &= -\beta_p. \end{aligned} \quad (9)$$

E. Multilayer-Layer Medium

Thanks to the piece-wise linear behavior of the SSP, we are now able to predict how a ray which starts from a given point, S, can travel through different layers to arrive at a specific point, E. Having built *ray patterns* using the above lemmas we can then for every P -part ray relate the ToF to the node's position using (6) for each single-layer part and the following boundary equations

$$\frac{X_{p+1} + Y_{p+1}}{1 - K_{p+1}} = \frac{X_p - Y_p}{1 + K_p}, \text{ for } p = 1 \text{ to } P - 1. \quad (10)$$

Note that, for each P -part ray between the points S and E, we have $E = E_P$, and $S = S_1$. The combination of the above equations forms a set of polynomial equations, and all the valid roots of this set of equations represent valid P -part paths between the two points. The ToF for any possible P -part ray can then be computed as

$$t = \sum_{p=1}^P \frac{-1}{a_p} \left[\ln \frac{1 + \sin \theta_p^E}{\cos \theta_p^E} - \ln \frac{1 + \sin \theta_p^S}{\cos \theta_p^S} \right]. \quad (11)$$

3. UNDERWATER RANGING TECHNIQUES

To our best knowledge, the algorithm in [8] is the only available mathematical approach for inhomogeneous SSP underwater range estimation. In order to better understand this algorithm we shortly review it here. The horizontal range between two nodes at different depths in an underwater medium can be obtained by

$$t = \int_{z^S}^{z^E} \frac{1}{c(z)} \frac{1}{\sqrt{1 - [k_0 c(z)]^2}} dz, \quad 0 < k_0 < \min_z \frac{1}{c(z)}, \quad (12)$$

$$r^E - r^S = \int_{z^S}^{z^E} \frac{k_0 c(z)}{\sqrt{1 - [k_0 c(z)]^2}} dz, \quad (13)$$

where k_0 is a constant defined by Snell's law, t is the ToF between two nodes, and $r^E - r^S$ represents the horizontal distance between them. The estimation of the horizontal distance has two phases; first, by measuring the depth and ToF information, the value of k_0 can be computed numerically from (12), and second, by substitution of k_0 into (13), and taking the integral, the value of $r^E - r^S$ can be obtained. This method is really comprehensive since with any given SSP, the horizontal distance is computable. However, in an inhomogeneous medium, a ray trajectory is not always a monotonic function of the depth, and as a result, whenever a path between two nodes crosses a depth more than once, which is quite common, the above formulas are not valid anymore. In this case, either (12) has no answer for k_0 in the specified range, or the obtained answer is not valid.

A. Proposed Algorithm

Assume, at a specific depth, the ToF of the fastest ray is a monotonic function of the horizontal range. In other words, a propagating wave at a specific depth reaches the destination with a smaller horizontal distance faster. Then, using the ToF and depth measurements, we can find the horizontal distance through a root finding algorithm such as Newton's method or bisection. The Newton's method is very fast, but it requires the derivative of the ToF w.r.t. the horizontal distance which is hard to compute. The bisection method is robust, and it eventually finds the solution. However, it requires an upper and a lower bound on the horizontal distance. The lower bound can be set to zero, and the upper bound can be computed through multiplying the measured ToF by the maximum sound speed of the entire environment. In spite of the fact that other efficient numerical root-finding algorithms can also be used, we utilize the simple bisection algorithm for the results in the numerical section.

Algorithm 1 shows the steps of the proposed algorithm. In this algorithm, K and E are the user-defined limits on the conditional criteria that determine when the algorithm exits from the loop, r_{low} and r_{up} are the lower and the upper bound, respectively, and the hats indicate measured or estimated quantities. The algorithm starts by initializing the upper and the lower bound, and then it computes the fastest ToF for the midpoint of the bounds. In order to calculate the fastest ToF, given the depth of the two points, different ray-patterns that may host the fastest ray, are formed, and all the rays between the points are found and their corresponding ToFs are computed, i.e, in Algorithm 1, t_l represents the ToF of the l -th found ray between the points. Then, among all these ToFs, the smallest one is selected. Next, based on the computed ToF, the lower, the upper, or both bounds are modified accordingly, and the procedure continues until one of the conditional criteria of the loop fails.

B. Cramér Rao Bound

The Cramér-Rao bound (CRB) expresses a lower bound on the variance of any unbiased estimator of a deterministic parameter. In this section we only derive the CRB for the horizontal distance estimation between two nodes. For the computation of the horizontal distance, three measurements are required; two depth measurements which are not directly related to the horizontal distance, and one ToF measurement. It is assumed that all the measurements are affected by Gaussian distributed noise as

$$\begin{aligned}\hat{t} &= t + n_t, \\ \hat{z}^S &= z^S + n_z^S, \\ \hat{z}^E &= z^E + n_z^E,\end{aligned}\quad (14)$$

where n_t , n_z^S and n_z^E are independent Gaussian distributed with variance σ_t^2 , σ_z^S and σ_z^E , respectively. The Fisher information matrix for estimating the horizontal distance $(r^E - r^S)$, z^S , and

Algorithm 1 Proposed Algorithm

```

Compute horizontal distance upper and lower bounds,
 $r_{\text{low}} = 0$ ,
 $r_{\text{up}} = \hat{t}c_{\text{max}}$ , where  $c_{\text{max}} = \max_z c^{(j)}(z)$ ,  $j \in 1, \dots, N$ .
Initialize loop criteria,
 $e = r_{\text{up}} - r_{\text{low}}$ ,
 $k = 1$ .
while  $e \leq E$  and  $k \leq K$  do
  Compute the average value of the upper and the lower bound,
   $r = \frac{r_{\text{low}} + r_{\text{up}}}{2}$ .
  Find the smallest ToF for this horizontal distance, form all possible ray
  patterns hosting the fastest ray (see lemmas).
  Compute ToF for each possible ray  $t_l(r, \hat{z}_1^S, \hat{z}_P^E)$ , (see (11)).
  Select the ray with the smallest ToF.
   $t = \min_l t_l(r, \hat{z}^S, \hat{z}^E)$ .
  Update the lower or the upper bound,
  if  $t < \hat{t}$  then
     $r_{\text{low}} = r$ .
  else if  $t > \hat{t}$  then
     $r_{\text{up}} = r$ .
  else
     $r_{\text{low}} = r$ ,
     $r_{\text{up}} = r$ .
  end if
  Update loop criteria,
   $e_r = r_{\text{up}} - r_{\text{low}}$ ,
   $k = k + 1$ .
end while
Compute the estimated horizontal distance between the nodes.  $\hat{r}^E - \hat{r}^S =$ 
 $\frac{r_{\text{low}} + r_{\text{up}}}{2}$ .

```

z^E can be obtained as

$$\mathbf{I} = \frac{1}{\sigma_t^2} \begin{bmatrix} \frac{\partial t}{\partial(r^E - r^S)} \\ \frac{\partial t}{\partial z^S} \\ \frac{\partial t}{\partial z^E} \end{bmatrix} \begin{bmatrix} \frac{\partial t}{\partial(r^E - r^S)} \\ \frac{\partial t}{\partial z^S} \\ \frac{\partial t}{\partial z^E} \end{bmatrix}^T + \begin{bmatrix} 0 & 0 & 0 \\ 0 & \sigma_z^{-2} & 0 \\ 0 & 0 & \sigma_z^{-2} \end{bmatrix}. \quad (15)$$

In order to compute the partial derivative $\frac{\partial t}{\partial(r^E - r^S)}$, we modify the environment in such a way that we can compute the horizontal distance as an integral w.r.t. depth. In order to achieve this, we have to convert the horizontal distance and the ToF to monotonic functions of the depth. Therefore, a ray can not have maximum or minimum points on its trajectory w.r.t. the depth. Let's illustrate the proposed idea with an example. Assume that a ray has a maximum point on its trajectory. The ray angle is zero at this maximum point, and after that it changes sign. But, this sign change does not affect Snell's law, as it is related to the cosine of the ray angle. As a result, we can assume that the ray travels upward instead of downward as depicted in Fig. 2, but in a new environment. In this new environment the SSP of each imaginary region must be changed accordingly. For instance, Fig. 2 shows that the real SSP is flipped and repeated in the first and second imaginary regions, respectively. In other words, the SSPs of the imaginary regions follow the behavior of the modified ray trajectory.

Note that the above conversion can only be done after we compute the fastest ray, because only then we are able to locate the maximum and/or minimum points on the trajectory and build the new environment. Under this assumption, the relation of the horizontal distance to the ToF is similar to (12), hence we can utilize the same approach used in [8] to compute the

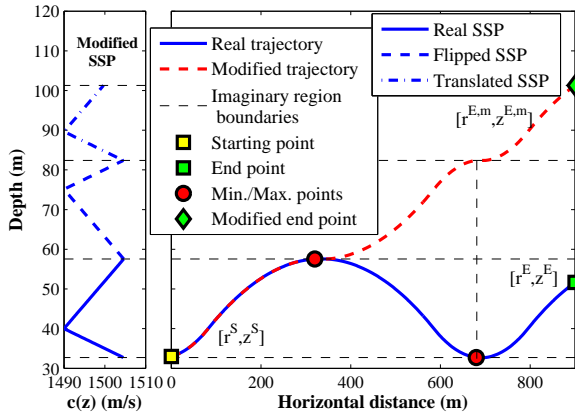


Fig. 2. Changing the real ray trajectory into a trajectory which is a monotonic function of the depth

CRB, which results into

$$\text{var}(\hat{r}^E - \hat{r}^S) \geq \sigma_t^2 \frac{1}{k_0^2} + \sigma_z^2 \frac{1 - (k_0 c(z^E))^2}{(k_0 c(z^E))^2} + \sigma_z^2 \frac{1 - (k_0 c(z^S))^2}{(k_0 c(z^S))^2}. \quad (16)$$

4. NUMERICAL RESULTS

We consider two kinds of SSP for our simulations which are shown in Fig 3; the former is derived from the sound speed measurements in the shallow water [9], and the latter is extracted from the sound speed of the Pacific Ocean and represents a deep water environment [6]. The procedure of finding the fastest path will be done in shallow water environment, and the proposed ranging algorithm will be evaluated in the deep underwater medium.

A. Ray Propagation for Shallow Water

Using the *ray pattern* concept, we are able to show how a ray can travel in a given medium, and which pattern may host the fastest ray. In Table. I, we show the family of patterns that a ray may travel between two points through different layers. These patterns are built based on the introduced lemmas. Since the depth of each node is known, we can select the proper patterns from the table, and form the corresponding polynomial formulas. By finding the roots of the polynomials, the ToF of each ray can be computed, and the fastest one will be recognized.

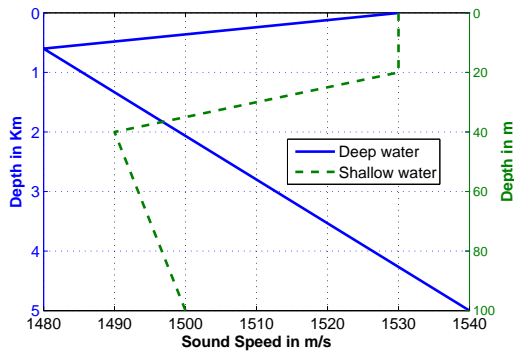


Fig. 3. Sound speed profile for deep and shallow water

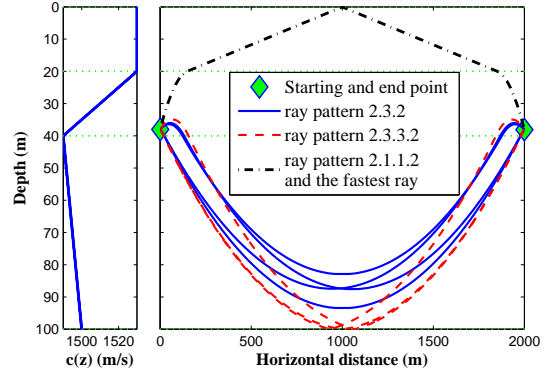


Fig. 4. Different possible rays between two points in the second layer

	to layer 1	to layer 2	to layer 3
	1	1.2	1.2.3
from layer 1		1.1.2 1.2.3.2	1.1.2.3 1.2.3.3
		1.2.3.3.2	1.2.3.2.3
from layer 2	2.1 2.1.1	2 2.1.1.2	2.3 2.1.1.2.3
		2.3.2	2.3.3
		2.3.2.3.2	2.3.2.3
		⋮	⋮
	3.2.1 3.3.2.1	3.2 3.2.1.1.2	3 3.3
from layer 3	3.3.2.1.1	3.2.3.2	3.2.3
		3.2.3.3.2	3.2.1.1.2.3
		3.2.3.2.3.2	3.2.3.2.3
		⋮	⋮

TABLE I
ALL POSSIBLE PATTERNS WHICH A FASTEST RAY IN A SHALLOW UNDERWATER ENVIRONMENT CAN FOLLOW

In Fig. 4, we show different possible rays that can travel between two points located in the second layer with a horizontal distance of 2000m. Based on the formulation, only three *ray patterns* can exist in this scenario, i.e., 2.3.2, 2.3.3.2, and 2.1.1.2 (here we only consider one reflection from the surface, and only one reflection from the floor in the existing ray patterns). Since the sound speed has higher values in the first and second layers, the fastest path belongs to the 2.1.1.2 pattern. In Table. I, we list different patterns which may host the fastest ray. In Fig. 5, we illustrate the analytical prediction of the fastest ray trajectory (only the crossing points are important) between two given points in the second layer. In order to find the fastest ray in the simulation part, the path trajectories of all rays departing the starting point are calculated, and the ones reaching the end point are selected. Then, among the selected rays, the one which has the lowest ToF is picked as the fastest ray. It is shown that the analytically calculated crossing points of the first arriving (fastest) ray with the layer boundaries matches perfectly the crossing points of the fastest ray found by the simulation. It is worth mentioning that the algorithm of [8] can not compute the correct horizontal range for any of the drawn blue-colored rays in Fig. 5 except for the first one, since all other ray trajectories are not monotonic functions of the depth.

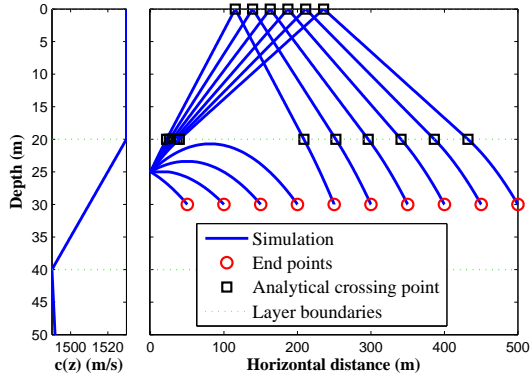


Fig. 5. Sample of ray propagation between two nodes

B. Ranging for Deep Water

In Fig. 6, we compare the performance of the proposed range algorithm with the one introduced in [8], and with the algorithms which approximate the inhomogeneous underwater medium as a homogeneous one with a presumably constant sound speed, i.e., the average sound speed of the two nodes' location. In this simulation, we consider Gaussian noise for the ToF and depth measurements with a standard deviation (std.) of $\sigma_t = 1\text{ms}$ and $\sigma_z = 1\text{m}$, respectively. In addition, we choose the deep water environment as a communication medium. The communication is between two points from different layers which are located at depth 500m and 700m, respectively. The root mean squared error (RMSE) for the horizontal estimation is computed by averaging over 1000 Monte Carlo simulations. As illustrated in this figure, the proposed algorithm performs well for all ranges while the algorithm of [8] has no definite solution from a given point as the horizontal range exceeds a given value. Furthermore, the straight-line algorithm degrades as the distance between the points increases.

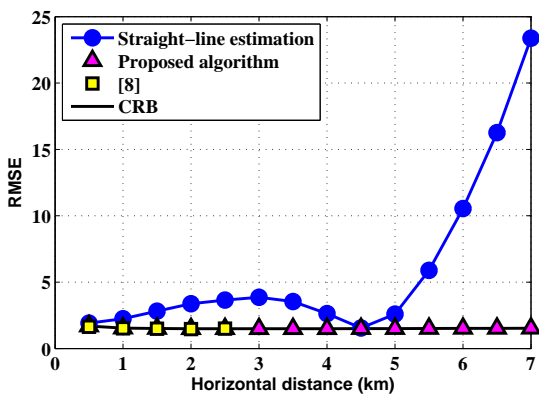


Fig. 6. Performance of the proposed algorithm for deep water

In Fig. 7, we investigate the effect of the measurement noise on the algorithms under consideration. Here the depth of the two nodes is as before, and their horizontal range is fixed at 6km. The horizontal axis represents how noisy the measured data are. The depth and ToF measurement noise powers are exponentially related to the parameter λ , i.e., $\sigma_z =$

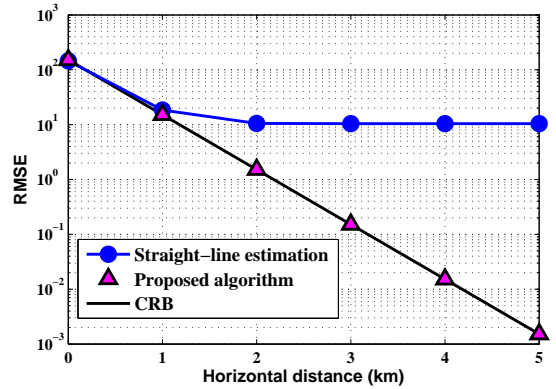


Fig. 7. Performance of the proposed algorithm for difference values of noise power

$10^3\sigma_t = 10^{2-\lambda}$. It can be seen that, the performance of the proposed ranging algorithm constantly improves and attains the CRB when we increase the measurement accuracy, while the straight-line estimation does not show any improvement after a given noise power.

5. CONCLUSIONS

We analyzed the problem of localizing a target node in an underwater environment. The inhomogeneous underwater medium upsets the linear dependency of the pair-wise distances to the time of flight. We showed that, if the depth information of the unlocalized node is available, then the problem of underwater localization can be converted to the traditional range-based one. Dividing the underwater medium into several isogradient sound speed profile layers, we completely analyzed how a ray can travel between two given points. Then, we proposed an iterative algorithm for the range estimation between two nodes, and we showed that the proposed algorithm attains the CRB and performs superb in comparison with other existing algorithms.

REFERENCES

- [1] M. Erol-Kantarci, H. T. Mouftah, and S. Oktug, "A survey of architectures and localization techniques for underwater acoustic sensor networks," *IEEE Communications Surveys and Tutorials*, appeared for publication, 2011.
- [2] S. Gerritsen, *Waves in Inhomogeneous Media*. PhD thesis, TU Delft, March. 2007.
- [3] A. Y. Teymorian, W. Cheng, L. Ma, X. Cheng, and X. Lu, "3D underwater sensor network localization," *IEEE Transactions on Mobile Computing*, vol. 8, pp. 1610–1621, May 2009.
- [4] G. Casalino and A. Caiti, "Rt²: A real-time ray-tracing method for acoustic evaluations among cooperating auvs," *Proc. IEEE OCEANS*, pp. 1–8, May 2010.
- [5] N. H. Kussat, C. D. Chadwell, and R. Zimmerman, "Absolute positioning of an autonomous underwater vehicle using GPS and acoustic measurements," *Oceanic Engineering, IEEE Journal of*, pp. 153 – 164, Jan. 2005.
- [6] M. B. Porter, "Acoustic models and sonar systems," *Oceanic Engineering, IEEE Journal of*, vol. 18, pp. 425–437, Oct. 1993.
- [7] H. Ramezani, H. J. Rad, and G. Leus, "Localization and tracking of a mobile target for an isogradient sound speed profile," *to appear, International Conference on Communications, ICC2012*.
- [8] C. R. Berger, S. Zhou, P. Willett, and L. Liu, "Stratification effect compensation for improved underwater acoustic ranging," *IEEE Transactions on Signal Processing*, vol. 56, pp. 3779–3783, Aug. 2008.
- [9] P. Gerstoft and W. S. Hodgkiss, "Effect of ocean sound speed uncertainty on matched-field geoacoustic inversion," *Acoustical Society of America*, June 2008.